CrossMark
click for updates

# Definitive proof of graphene hydrogenation by Clemmensen reduction: use of deuterium labeling†

Zdeněk Sofer,*[a] Ondřej Jankovský,[a] Alena Libánská,[a] Petr Šimek,[a] Michal Nováček,[a] David Sedmidubský,[a] Anna Macková,[b,c] Romana Mikšová[b,c] and Martin Pumera*[d]

Graphane is one of the most intensively studied derivatives of graphene. Here we demonstrate the evaluation of exact degree of graphene hydrogenation using the Clemmensen reduction reaction and deuterium labeling. The Clemmensen reduction reaction is based on application of zinc in an acid environment. It effectively reduces various functional groups (like ketones) present in graphite oxide. However, the mechanism of reduction is still unknown and elusive. Here we bring a major insight into the mechanisms of the Clemmensen reduction *via* deuterium labeling and the topochemical approach applied on graphite oxide. The use of deuterated reactants and the exact measurement of deuterium concentration in reduced/hydrogenated graphene by nuclear methods can be used for accurate estimation of C−H bond abundance in graphene. Various topochemical configurations of experiments showed that the reduction of a ketonic group proceeds in contact with the zinc metal by a carbenoid mechanism. Our results showed that the application of nuclear methods of isotope analysis in combination with deuterium labeling represents a very effective tool for investigation of graphene based materials. Our results demonstrate that graphene based materials can also be effectively used for the investigation of organic reaction mechanisms, because the robust structure of graphene allows the use of various spectroscopic techniques which could not be applied on small organic molecules.

## Introduction

Graphene and its chemical derivatives have been in the forefront of material research during the last decade.[1–4] Great interest is focused on the hydrogenated derivative of graphene–graphane.[5–7] This material belongs to a wide-bandgap semiconductor while maintaining the 2-dimensional structure of graphene.[6] Several possible applications of this material have been reported manifesting a huge application potential in micro- and optoelectronics, sensor devices and electrochemical energy storage and conversion devices.[8–10]

Recently several procedures for the synthesis of hydrogenated graphene have been reported. These methods are based on application of hydrogen plasma,[11,12] hydrogen treatment at elevated pressure[13] and reaction of solvated electrons with a proton source in the presence of graphene or some of its derivatives. The latter is typically based on the reaction of water or alcohol with the suspension of graphene or graphite in liquid ammonia containing a dissolved alkali metal.[14,15] Another method for graphane synthesis is the reduction of graphite oxide in the presence of an acid and an electropositive metal. This reaction is known from organic chemistry as the Clemmensen reduction.[16]

The Clemmensen reduction is applied in organic synthesis for the reduction of ketone groups to methylene groups.[17,18] The use of zinc in a hydrochloric acid environment has been used for the synthesis of chemically reduced graphene.[7,19] Such a reduction is believed to be accompanied by graphene hydrogenation; however, the proof of hydrogenation is based only on indirect evidence and without exact determination of the hydrogenation degree. Even though this reduction method dates to early decades of the last century, the reaction mechanism has not yet been described.[16] The reaction proceeds typically in the presence of zinc (or zinc activated by amalga-

[a]*Department of Inorganic Chemistry, University of Chemistry and Technology, Prague 166 28 Prague 6, Czech Republic. E-mail: zdenek.sofer@vscht.cz; Fax: +420 22431-0422*
[b]*Nuclear Physics Institute of the ASCR, v. v. i., 250 68 Řež, Czech Republic. E-mail: mackova@ujf.cas.cz*
[c]*Department of Physics, Faculty of Science, J.E. Purkine University, 400 96 Ústí nad Labem, Czech Republic*
[d]*Division of Chemistry & Biological Chemistry, School of Physical and Mathematical Sciences, Nanyang Technological University, Singapore, 637371, Singapore. E-mail: pumera@ntu.edu.sg; Fax: +65 6791-1961*
†Electronic supplementary information (ESI) available. See DOI: 10.1039/c5nr01356a

mation) in hydrochloric acid. For the reaction mechanism two pathways have been generally suggested. In the case of the 'carbanionic mechanism' the zinc ion attacks the protonated carbonyl directly in the solution, while in the 'carbenoid mechanism' the reduction takes place on the surface of the zinc metal and this reaction has a radical nature.

To investigate the role of Zn in the Clemmensen reduction process, we applied this process on different graphite oxides (GOs) using hydrochloric acid and deuterated hydrochloric acid to investigate the reaction mechanism.[20–23] The reaction of a metal with an acid leads to hydrogen evolution and a strongly reducing environment is formed. However, the existence and properties of the evolved active hydrogen are still questioned in the literature. We show here that the reduction takes place only in contact with the zinc metal while the role of active hydrogen in the reaction is only marginal. We used the graphite oxide (GO) as a model substrate, since it represents a suitable system for the application of a topochemical approach (various arrangements of experimental geometry and rigid substrates suitable for reactions – graphite oxide) and also novel analytical methods can be applied which are not suitable for small molecules. Note that GO is not an "oxide" in the standard chemical sense since it contains a large variety of oxygen containing groups, predominantly epoxy, hydroxyl and ketone groups.[24] The oxygen containing groups of GO have been often used as components for covalent functionalization.[25] However, to the best of our knowledge, there have not yet been any efforts to examine the reaction mechanism using GO. Our observations bring new insight into the mechanism of the Clemmensen reaction and demonstrate the synthesis of hydrogenated and deuterated graphene with various degrees of C/H and C/D ratios, respectively.

## Experimental

### Materials

We used pure graphite microparticles (2–15 μm, 99.9995%, from Alfa Aesar). Sulfuric acid (98%), nitric acid (68%), fuming nitric acid (>98%), potassium chlorate (99%), potassium permanganate (99.5%), sodium nitrate (99.5%), hydrogen peroxide (30%), hydrochloric acid (37%), silver nitrate (99.5%), barium nitrate (99.5%) and N,N-dimethylformamide (DMF) were obtained from Penta, Czech Republic. Deuterium chloride (35% in $D_2O$, >98% D), deuterium oxide (99.9% $D_2O$) and Zn powder were obtained from Sigma-Aldrich, Czech Republic.

### Synthesis procedure

We prepared four different graphite oxides by four most common methods: Hofmann (HO-GO), Hummers (HU-GO), Brodie (BR-GO) and Staudenmaier (ST-GO).[20–23]

(1) HO-GO. Sulfuric acid (98%, 87.5 mL) and nitric acid (68%, 27 mL) were added to a reaction flask (Pyrex beaker with thermometer) containing a magnetic stir bar. The mixture was then cooled by immersing in an ice bath for 30 min. Graphite (5 g) was then added to the mixture with vigorous stirring.

While keeping the reaction flask in the ice bath, potassium chlorate (55 g) was slowly added to the mixture. Upon the complete dissolution of potassium chlorate, the reaction flask was then loosely capped to allow the gas evolved to escape and the mixture was continuously stirred for 96 hours at room temperature. The mixture was poured into 3 L of deionized water and decanted. Graphite oxide was then redispersed in HCl solution (5%, 3 L) to remove the sulfate ions and repeatedly centrifuged and redispersed in deionized water until a negative reaction on chloride and sulfate ions was achieved. The graphite oxide slurry was then dried in a vacuum oven (50 °C, 48 hours).

(2) HU-GO. Graphite (5 g) and sodium nitrate (2.5 g) were stirred with sulphuric acid (98%, 115 mL). The mixture was then cooled to 0 °C. Potassium permanganate (15 g) was then added over a period of two hours. During the next four hours, the reaction mixture was allowed to reach room temperature before being heated to 35 °C for 30 min. The reaction mixture was then poured into a flask containing deionized water (250 mL) and heated to 70 °C for 15 minutes. The mixture was then poured into deionized water (1 L). The unreacted potassium permanganate and manganese dioxide were removed by the addition of 3% hydrogen peroxide. The reaction mixture was then allowed to settle and decanted. The obtained graphite oxide was then purified by repeated centrifugation and redispersing in deionized water until a negative reaction on sulphate ions was achieved. Graphite oxide slurry was then dried in a vacuum oven (50 °C, 48 hours).

(3) BR-GO. Fuming nitric acid (>98%, 62.5 mL) was added to a reaction flask containing a magnetic stir bar. The mixture was then subsequently cooled to 0 °C and then graphite (5 g) was added. The mixture was stirred to obtain a homogeneous dispersion. While keeping the reaction flask at 0 °C, potassium chlorate (25 g) was slowly added to the mixture. Upon the complete dissolution of potassium chlorate, the reaction flask was loosely capped to allow the gas evolved to escape and the mixture was stirred for 20 h at 40 °C. Upon the completion of the reaction, the mixture was poured into 3 L of deionized water and decanted. Graphite oxide was then redispersed in HCl solution (5%, 3 L) to remove sulphate ions and repeatedly centrifuged and redispersed in deionized water until a negative reaction on chloride ions was achieved. The graphite oxide slurry was then dried in a vacuum oven (50 °C, 48 hours).

(4) ST-GO. Sulphuric acid (98%, 87.5 mL) and fuming nitric acid (>98%, 27 mL) were added to a reaction flask containing a magnetic stir bar. Subsequently, the mixture was cooled to 0 °C and then graphite (5 g) was added. The mixture was vigorously stirred to avoid agglomeration and to obtain a homogeneous dispersion. While keeping the reaction flask at 0 °C, potassium chlorate (55 g) was slowly added. Upon the complete dissolution of potassium chlorate, the reaction flask was loosely capped to allow the gas evolved to escape. Then the mixture was continuously stirred for 96 h at room temperature. The mixture was then poured into deionized water (3 L) and decanted. Graphite oxide was redispersed in HCl solution (5%, 3 L) to remove sulphate ions and repeatedly centrifuged and

redispersed in deionized water until a negative reaction on chloride and sulphate ions was achieved. The graphite oxide slurry was then dried in a vacuum oven (50 °C, 48 hours).

For the reduction 100 mg of GO was dispersed in $H_2O$ and $D_2O$, respectively, by ultrasonication (400 W, 30 minutes). 10 mL of concentrated HCl or DCl and 2.5 g of zinc powder were then added to the dispersion. The reaction mixture was vigorously stirred for 24 hours. In the case of $D_2O$/DCl the reduction was performed under an argon atmosphere. Reduced graphene was separated by suction filtration and washed with diluted hydrochloric acid (1 : 10 by vol.) and deionized water. Reduced graphene was dried in a vacuum oven (60 °C, 48 hours) prior to the further use.

### Analytical techniques

The morphology was investigated by scanning electron microscopy (SEM) with an FEG electron source (Tescan Lyra dual beam microscope). Elemental composition and mapping were performed using an energy dispersive spectroscopy (EDS) analyzer (X-Max[N]) with a 20 mm² SDD detector (Oxford Instruments) and AZtecEnergy software. To conduct these measurements, the samples were placed on a carbon conductive tape. SEM and SEM-EDS measurements were carried out using a 10 kV electron beam.

Raman spectroscopy was conducted on an InVia Raman microscope (Renishaw, England) with a CCD detector in backscattering geometry. A DPSS laser (532 nm, 50 mW) with a 100× magnification objective was used for the Raman measurements. The instrument was calibrated with a silicon reference to give a peak position at 520 cm⁻¹ and a resolution of less than 1 cm⁻¹.

Combustible elemental analysis (CHNS-O) was performed using a PE 2400 Series II CHNS/O Analyzer (Perkin Elmer, USA). The instrument was used in CHN operating mode (the most robust and interference-free mode) to convert the sample elements to simple gases ($CO_2$, $H_2O$ and $N_2$). The PE 2400 analyzer automatically performed combustion, reduction, homogenization of the product gases, separation and detection. An MX5 microbalance (Mettler Toledo) was used for precise weighing of the samples (1.5–2.5 mg per single sample analysis). Using this procedure, the accuracy of CHN determination is better than 0.30% abs. Internal calibration was performed using an N-phenyl urea.

Fourier transform infrared spectroscopy (FTIR) measurements were performed on a NICOLET 6700 FTIR spectrometer (Thermo Scientific, USA). A diamond ATR crystal and DTGS detector were used for all measurements, which were carried out in the range 4000–400 cm⁻¹.

High resolution X-ray photoelectron spectroscopy (XPS) was performed using an ESCAProbeP spectrometer (Omicron Nanotechnology Ltd, Germany) with a monochromatic aluminium X-ray radiation source (1486.7 eV). The samples were placed on a conductive carbon tape homogeneously covered with the sample.

For the measurement the samples were compressed in the form of pellets (1/4″ diameter, 1 mm thickness). The RBS and

ERDA measurements were performed using a tandem accelerator Tandetron 4130 MC (High Voltage Engineering Europa B.V., Netherland). The RBS measurement was performed with 2 MeV He⁺ ions (for C, O and S) and 3.716 MeV He⁺ ions (for N). The measurement geometry uses 0° entrance angle and 170° scattering angle. The ERDA measurement was performed with 2.5 MeV He⁺ ions (75° entrance angle and 30° scattering angle). Backscattered ions were detected using an ULTRA ORTEC detector placed below the entrance beam (Cornell geometry). A Canberra PD-25-12-100 AM detector placed in the plane with the entrance beam (IBM geometry, 12 μm Mylar foil for the elimination of He⁺ and heavier ions) was used for the detection of forward scattered ions. The obtained spectra were evaluated using SIMNRA 6.06 and GISA 3.99 software.[26,27]

## Results and discussion

The reduction was performed by zinc dust using aqueous suspension of GO in 1 M hydrochloric acid.[4–7] For the synthesis of deuterium labeled graphenes 1 M deuterium chloride in $D_2O$ was used. The whole experimental procedure is described in detail in the Experimental section. The samples reduced with zinc suspension in acid are named HO/H/Zn, HO/D/Zn, HU/H/Zn, HU/D/Zn, ST/H/Zn and BR/H/Zn. The first two letters indicate the method of graphite oxide synthesis (HO – Hofmann, HU – Hummers, ST – Staudenmaier, BR – Brodie), while the second part of the notation indicates whether the reduction was performed in $H_2O$/HCl (marked as H) or in $D_2O$/DCl (marked as D).

We also carried out the reduction of selected graphite oxide (HO-GO) in two different experimental configurations – in the direct contact with zinc and only in the contact with the formed "nascent" hydrogen. The advantage of GO as a substrate is that we can employ "topochemical" reactions. Indeed, performing the chemical reaction on a rigid substrate formed by graphite oxide which is brought into contact with zinc as a reducing agent makes it possible to explore various geometries of experimental configuration. Moreover the rigid substrate is suitable for further characterization by analytical methods which could not be applied on small molecules because these freely migrate in the solution and thus one cannot pinpoint whether "nascent" hydrogen plays an active role or the presence of the Zn surface is crucial. The process of reduction is illustrated in Scheme 1.
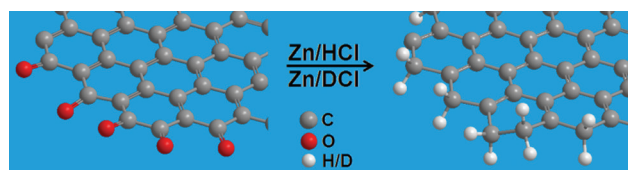


Scheme 1 The process of graphite oxide hydrogenation via Clemmensen reduction reaction.

**Table 1** The composition of graphite oxides exposed to Clemmensen reduction under different conditions (HCl/DCl) by elemental combustion analysis in at%

| Sample | N | C | H | O | O–H |
|--------|------|-------|-------|-------|-------|
| HO/H/Zn | 0 | 37.86 | 37.91 | 24.23 | 13.68 |
| HO/D/Zn | 0.06 | 39.45 | 34.15 | 26.33 | 7.82 |
| HU/H/Zn | 0.12 | 80.43 | 11.48 | 7.97 | 3.51 |
| HU/D/Zn | 0.03 | 80.65 | 10.7 | 8.62 | 2.08 |
| BR/H/Zn | 0.29 | 48.8 | 29.7 | 21.21 | 8.49 |
| ST/H/Zn | 0.19 | 72.95 | 13.68 | 13.17 | 0.51 |

The total concentrations of C, H, N and S were obtained by the elemental combustion analysis (Table 1). Based on these results we can calculate the minimal concentration of C–H bonds by a simple subtraction of hydrogen and oxygen concentration in atomic percent. In the oxygen functional groups the possible H/O ratio is 1 for hydroxyl groups, 0.5 for carboxylic acids and 0 for ketonic and epoxide groups. The highest difference between C and H and therefore the highest concentration of C–H bonds, 13.68 at%, was observed for HO/H/Zn, while the lowest concentration of C–H groups was found in ST/H/Zn. A slightly lower concentration of hydrogen measured for deuterated samples originates from the different atomic mass of hydrogen and deuterium resulting in lower concentration of hydrogen observed by elemental combustion analysis. This is in good agreement with the mechanism based on the Clemmensen reduction where ketonic groups are reduced/hydrogenated and C–H bonds are formed. Graphite oxide surface typically contains also an appreciable amount of aldehyde and epoxide groups which undergo reduction. Particularly the epoxide groups are quite reactive and their reduction led to epoxide ring opening and a simultaneous formation of C–H and C–OH groups on the reduced graphene surface.

The sample morphology was investigated by scanning electron microscopy (SEM). Images taken at different magnifications are shown in Fig. 1. The morphology of the prepared materials is typical for reduced and exfoliated graphite oxide. As expected, no significant differences were observed between the individual samples.
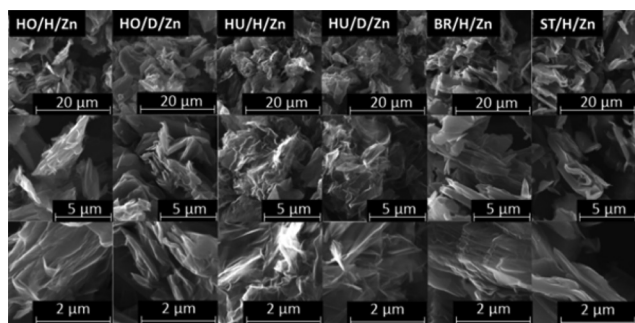


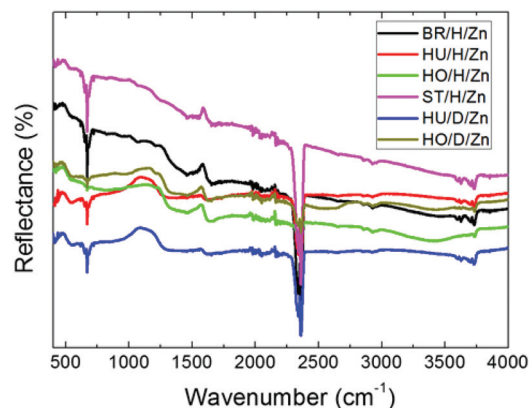**Fig. 1** SEM micrographs of reduced graphite oxides.



**Fig. 2** FT-IR spectra of graphite oxides exposed to Clemmensen reduction under different conditions (HCl/DCl).

The presence of C–H bonds was also proved by FT-IR spectroscopy (Fig. 2). The FT-IR spectra of the starting graphite oxides are shown in Fig. S1.† The weak effects located at 2900 cm$^{-1}$ and 2950 cm$^{-1}$ are indicative of C–H and C–H$_2$ groups in the reduced/hydrogenated GO. The spectra acquired for HO-GO and HU-GO reduced in normal or deuterated hydrochloric acid exhibit an almost identical shape suggesting a similar reaction product. Also the C=C bond from the graphene skeleton, represented by a peak at 1540 cm$^{-1}$ and a broad band around 1200 cm$^{-1}$ from remaining hydroxyl groups (C–O vibration band), were detected.

The quality of material from the point of view of defects and the presence of sp$^3$ bonded carbon were investigated using Raman spectroscopy (Fig. 3). The most significant is the presence of D and G bands located at 1360 cm$^{-1}$ and 1560 cm$^{-1}$, respectively.[28] The intensity of the D band is correlated with the presence of defects and carbon in sp$^3$ hybridization. The G band is associated with sp$^2$ hybridized carbon in the graphene planar sheet. D/G ratios were calculated from Raman spectra to compare the defect density (Table 2). The clear correlation between the degree of oxidation of the starting graphite oxide and D/G ratios was observed. The starting graphite oxide with the highest degree of oxidation (HU-GO) also exhibits the highest D/G ratio. Slight differences in higher D/G ratios for samples hydrogenated with hydrogen can be related to the weak isotopic effect where generally heavier deuterium containing molecules have lower reaction rates compared to hydrogen. However, due to very low differences no clear evidence of the hydrogen/deuterium kinetic effect was found. The average crystallite size $L_a$ was also calculated from D/G ratios using the equation:[29]

$$L_a = 2.4 \times 10^{-10} \times \lambda_{laser}^4 \times I_G/I_D \quad (1)$$

where $I_G$ and $I_D$ denote the respective intensities of the G and D peaks and $\lambda_{laser}$ is the wavelength of the laser used in nm (Table 2).

The most suitable method to verify the presence of C–H bonds is the direct measurement of deuterium concentration
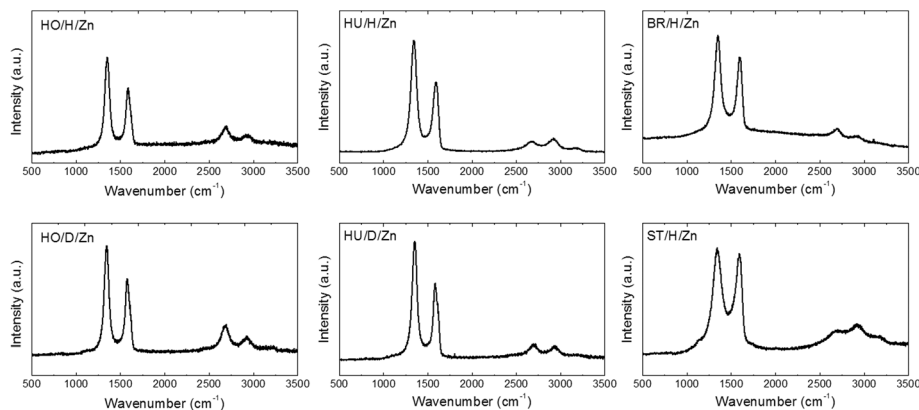
**Fig. 3** Raman spectra of reduced graphite oxides.

**Table 2** D/G ratios and corresponding crystallite sizes

| Sample | D/G | Cryst. size (nm) |
| --- | --- | --- |
| HO/H/Zn | 1.4 | 13.7 |
| HO/D/Zn | 1.37 | 14 |
| HU/H/Zn | 1.56 | 12.3 |
| HU/D/Zn | 1.5 | 12.8 |
| BR/H/Zn | 1.23 | 15.6 |
| ST/H/Zn | 1.05 | 18.3 |

in the samples synthesized by reduction of graphite oxide in deuterated hydrochloric acid. This experiment was performed using a combined nuclear method of Rutherford backscattering (RBS) and elastic recoil detection analysis (ERDA) (Fig. 4). The combination of these two techniques allowed us not only to detect basic elemental composition of light elements (C, H, N) but also to distinguish and quantify the concentration of hydrogen and deuterium within the samples (Table 3).

The concentration of deuterium was higher in HO/D/Zn (10.8 at%) compared to HU/D/Zn (4.2 at%). This is in good agreement with elemental combustion analysis where the highest concentration of C–H bonds was supposed for samples prepared from HO-GO. The higher concentration of C–D bonds in HO/D/Zn can be explained in terms of radical opening of the epoxide ring which led to simultaneous formation of C–D and C–OD bonds. In order to prove that deuterium is present only in the form of C–D bonds and as a part of oxygen functional groups (C–OD), the samples were repeatedly washed with normal water and hydrochloric acid after the reaction. The gradient of hydrogen/deuterium concentration led to an exchange of acidic deuterium (present in –C–OD and –COOD groups) with hydrogen and only the C–D bond remained unaffected. HO-GO contained a high concentration of reactive oxygen functional groups which undergo reduction/hydrogenation with zinc in an acidic environment. This led us to a conclusion that the presence of epoxide and ketone groups is the most important factor for the hydrogenation.

To get a deeper insight into the chemistry of reduced/hydrogenated graphene we applied high resolution X-ray photoelectron spectroscopy (XPS). A wide range scan was used to obtain the concentration of carbon, oxygen and the C/O ratio which indicates the degree of reduction. The dominant peaks are C 1s at 284.5 eV and O 1s at 532.5 eV (Fig. 5). The XPS survey spectra of the starting graphite oxides and the corresponding high resolution XPS spectra are shown in the ESI (Fig SI3†). The composition of the starting graphite oxides obtained by XPS is shown in Table SI3.† The minor F 1s peak (at 689 eV) originated from vacuum grease used during synthesis; however, no fluorine was detected by elemental combustion analysis. This indicates that the contamination was present only on the surface. The highest C/O ratios were obtained for HU/H/Zn (16.2) and for HU/D/Zn (14.2). Comparing these results with Raman spectroscopy data, we can conclude that the high D/G ratio originated mostly from defects induced by reduction. A relatively high C/O ratio was determined for ST/H/Zn (12.2). The lowest values of C/O ratios were obtained for HO/H/Zn (8.6), HO/D/Zn (9.9) and BR/H/Zn (8.8). The results of XPS analysis are summarized in Table 4. Let us note that such a high C/O ratio is comparable with the thermally reduced graphene and is significantly higher than typical values observed on chemically reduced graphene.[30]

The deconvolution of the C 1s peak was performed to obtain information about bonding conditions and relative concentration of individual functionalities (Fig. 6). Six different carbon bonds were assumed: the C=C (284.5 eV), the C–C/C–H (285.5 eV), the C–O of alcohol/ether groups (286.3 eV), the C=O of carbonyl groups (288 eV), O–C=O of carboxylic acid/ester groups (289 eV) and the π–π* interactions (291 eV). The results of deconvolution for C 1s are shown in Table 5. Only small differences were identified between the respective samples which indicates a similar reduction mechanism with hydrogen and deuterium without any significant isotopic kinetic effect. The peak at 285.5 eV is attributed to both the C–H and C=C bonds due to their similar energies, therefore this XPS cannot give an exact evidence of the C–H bond. The high degree of reduction was also documented by high resolu-
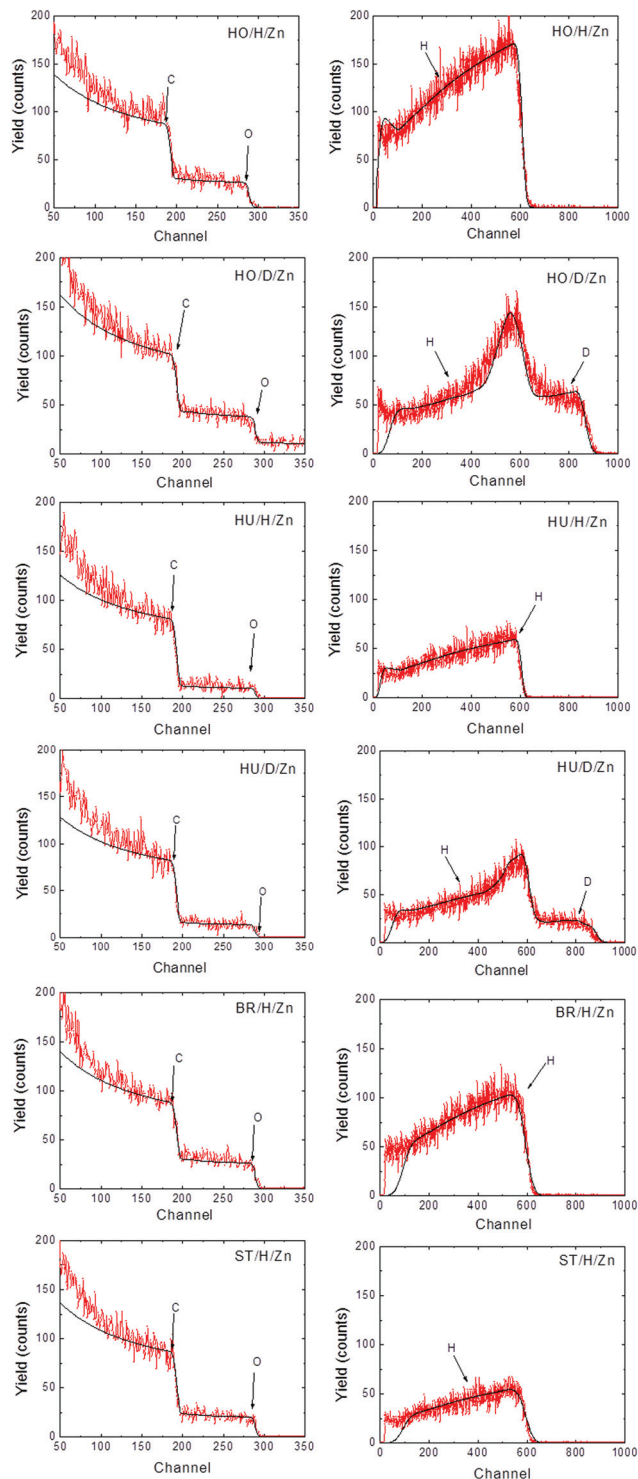
**Fig. 4** Rutherford backscattering (left) and elastic recoil detection analysis (right). Red lines represent the experimental data while the simulated profiles are depicted in black.

**Table 3** The composition of graphite oxides exposed to Clemmensen reduction under different conditions (HCl/DCl) by Rutherford backscattering and elastic recoil detection analysis in at%

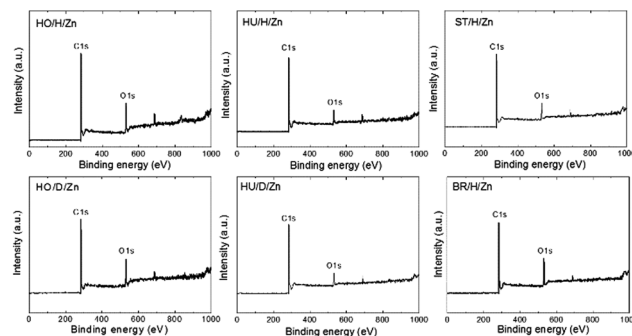| Sample | C | O | H | D |
|---|---|---|---|---|
| HO/H/Zn | 64.5 | 16.1 | 19.4 | 0.0 |
| HO/D/Zn | 67.8 | 17.1 | 3.9 | 10.8 |
| HU/H/Zn | 83.0 | 7.1 | 9.9 | 0.0 |
| HU/D/Zn | 80.0 | 8.9 | 6.9 | 4.2 |
| BR/H/Zn | 66.3 | 16.5 | 17.2 | 0.0 |
| ST/H/Zn | 76.9 | 13.6 | 9.5 | 0.0 |



**Fig. 5** XPS survey spectra of graphite oxides exposed to Clemmensen reduction under different conditions (HCl/DCl).

**Table 4** The composition of graphite oxides exposed to Clemmensen reduction under different conditions (HCl/DCl) by XPS in at%

| Sample | C | O | C/O |
|---|---|---|---|
| HO/H/Zn | 89.6 | 10.4 | 8.6 |
| HO/D/Zn | 90.8 | 9.2 | 9.9 |
| HU/H/Zn | 94.2 | 5.8 | 16.2 |
| HU/D/Zn | 93.4 | 6.6 | 14.2 |
| BR/H/Zn | 92.4 | 7.6 | 12.2 |
| ST/H/Zn | 89.8 | 10.2 | 8.8 |

In order to resolve the mechanism of the Clemmensen reduction we applied various geometrical arrangements of the substrate (graphite oxide) and the reducing agent (zinc). This could not be applied for simple small molecules in a solution, but the large graphene sheets can be arranged in various experimental configurations and subsequently analyzed by different characterization techniques. We performed two different experiments. For the first experiment we placed HO-GO in direct contact with the metal (sample was termed HO–C) while for the second one HO-GO was kept away from the metal, where only active (nascent) hydrogen formed by dissolution of zinc came into contact with HO-GO (sample was termed HO–N). These samples were analyzed by various methods after four hours in reaction environment.

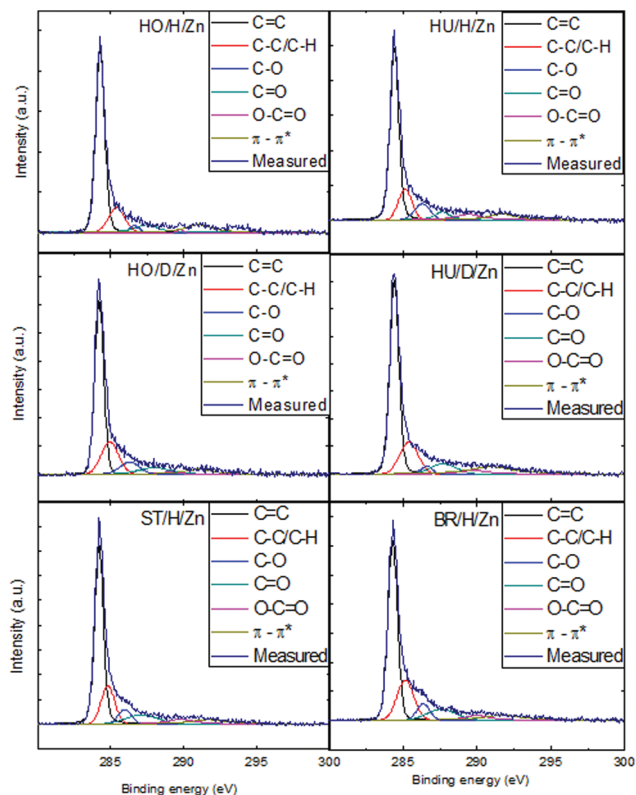To examine the reduction of the C=O functional group FT-IR measurement was performed for HO–C and HO–N and

tion O 1s spectra where only single peak at 532.5 eV correlated with the C–O bond is dominantly present after reduction (Fig. S2†).

Fig. 6 The deconvolution of C 1s peak of graphite oxides exposed to Clemmensen reduction under different conditions (HCl/DCl).
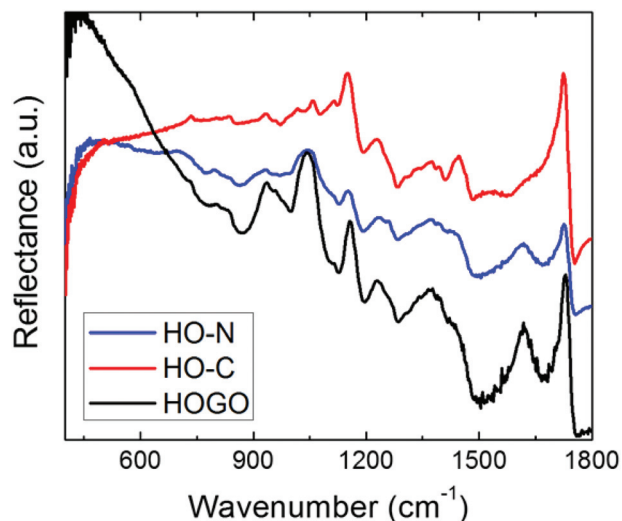


Fig. 7 FT-IR spectra of starting graphite oxide (HO-GO) and HO-GO reduced in contact (HO−C) and without contact with zinc metal (HO−N).
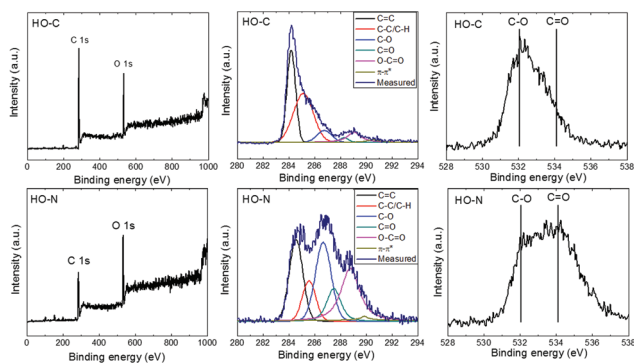


Fig. 8 XPS survey spectra (left), fitted high resolution C 1s peak (middle) and O 1s peak (right) of GO reduced in contact with Zn (C) and without the direct contact with the Zn metal (N).

Table 5 The different bonding arrangements in graphite oxides exposed to Clemmensen reduction under different conditions (HCl/DCl) based on HR-XPS analysis by deconvolution of the C 1s peak (%)

| Sample | C=C | C–C/C–H | C–O | C=O | O–C=O | $\pi-\pi^*$ |
|---|---|---|---|---|---|---|
| HO/H/Zn | 62.7 | 14 | 2.3 | 9.4 | 0.6 | 11 |
| HO/D/Zn | 54.1 | 18.6 | 8.8 | 8.8 | 2.1 | 7.6 |
| HU/H/Zn | 55.6 | 13.7 | 8.6 | 6.1 | 7.7 | 8.3 |
| HU/D/Zn | 55 | 16.8 | 2.5 | 7.4 | 4.5 | 13.8 |
| ST/H/Zn | 54.5 | 16.2 | 6 | 8.5 | 6.6 | 8.2 |
| BR/H/Zn | 52.4 | 19.5 | 6.2 | 9.1 | 4.8 | 8 |

also for HO-GO (for the comparison) (Fig. 7). The significant reduction of C=O vibration band intensity (1630 cm$^{-1}$) is clearly visible for the HO-C sample. The vibration band originated from C–O vibration in OH groups remained almost unchanged (1290 cm$^{-1}$, 1190 cm$^{-1}$ and 1130 cm$^{-1}$). The vibration band originated from the C–O band of the epoxide ring is suppressed for both samples (1000 cm$^{-1}$ and 870 cm$^{-1}$) and indicates high reactivity of these functional groups in graphite oxide. The vibration band at ~1520 cm$^{-1}$ originated from the graphene skeleton. In contrast, HO−N still exhibits the band at energy 1630 cm$^{-1}$ confirming that the direct contact of the C=O group with Zn is required for the Clemmensen reduction to proceed.

The XPS analysis results showed significant differences between HO-C and HO−N (Fig. 8). On the O 1s peak we observed a nearly complete disappearance of the C=O bond for the HO–C sample. The same effect was identified for C 1s, where also a significant decrease of the C=O concentration was found compared to HO–N (see Table 6). This resulted in much higher C/O ratios for HO–C (4.8 for HO–C and 2.7 for HO–N). The C/O ratio in HO–N is almost identical with that of

Table 6 The C 1s peak deconvolution for samples HO−C (contact with Zn) and HO−N (no contact with Zn)

| Sample | C=C | C–C/C–H | C–O | C=O | O–C=O | $\pi-\pi^*$ |
|---|---|---|---|---|---|---|
| HO-C | 34.8 | 43.3 | 8.1 | 2.3 | 9.3 | 2.2 |
| HO-N | 23.2 | 11.2 | 26.5 | 10.5 | 25.4 | 3.1 |
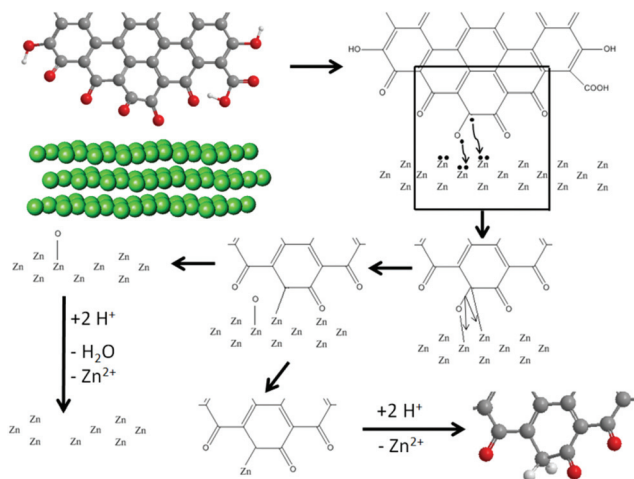
**Scheme 2** The mechanism of ketone group reduction on graphite oxide. The Zn atoms in the scheme mean zinc metal surface.

HO-GO (2.8) indicating almost negligible extent of reduction. A relatively high concentration of carboxylic acid functional groups on HO–C suggests that these functional groups are not affected by Zn/HCl reduction which is in agreement with reactions performed on small organic molecules.

These exceptionally interesting findings allowed us to conclude that the mechanism of the Clemmensen reduction should be based on the carbenoid mechanism. The following reaction scheme (Scheme 2) based on our observations illustrates the reduction of HO-GO in direct contact with zinc (sample HO–C).

## Conclusions

The reduction/hydrogenation of various graphite oxides by zinc in hydrochloric acid was investigated in detail. Deuterium labeling was applied to assess the exact degree of graphite hydrogenation. The amount of deuterium was estimated using nuclear methods of material analysis – RBS and ERDA. In addition, the topological approach was applied in order to identify the mechanism of graphite oxide reduction by zinc in an acidic environment – Clemmensen reduction. The results indicate that the reduction/hydrogenation of the ketonic groups proceeds only in contact with the surface of the zinc metal whereas the so called "nascent hydrogen" affects only the reduction of highly reactive oxygen functional groups such as epoxides. The combination of such analytic techniques allowed us to understand the role of Zn in the mechanism of the Clemmensen reduction and to exactly determine the degree of hydrogenation. In addition, this study is essential for future investigation of various reaction mechanisms, where a similar approach can be applied. Graphite oxide with higher concentration of ketone functional groups can be further applied for the synthesis of highly hydrogenated graphene or even pure graphane.

## Notes and references

1 A. K. Geim and K. S. Novoselov, *Nat. Mater.*, 2007, **6**, 183–191.
2 Z. Sofer, O. Jankovský, P. Šimek, K. Klímová, A. Macková and M. Pumera, *ACS Nano*, 2014, **8**, 7106–7114.
3 O. Jankovsky, P. Simek, D. Sedmidubsky, S. Matejkova, Z. Janousek, F. Sembera, M. Pumera and Z. Sofer, *RSC Adv.*, 2014, **4**, 1378–1387.
4 O. Jankovsky, P. Simek, K. Klimova, D. Sedmidubsky, S. Matejkova, M. Pumera and Z. Sofer, *Nanoscale*, 2014, **6**, 6065–6074.
5 D. Elias, R. Nair, T. Mohiuddin, S. Morozov, P. Blake, M. Halsall, A. Ferrari, D. Boukhvalov, M. Katsnelson and A. Geim, *Science*, 2009, **323**, 610–613.
6 J. O. Sofo, A. S. Chaudhari and G. D. Barber, *Phys. Rev. B: Condens. Matter*, 2007, **75**, 153401.
7 Z. Sofer, O. Jankovsky, P. Simek, L. Soferova, D. Sedmidubsky and M. Pumera, *Nanoscale*, 2014, **6**, 2153–2160.
8 T. Hussain, B. Pathak, T. A. Maark, C. M. Araujo, R. H. Scheicher and R. Ahuja, *EPL*, 2011, **96**, 27013.
9 M. Pumera and C. H. A. Wong, *Chem. Soc. Rev.*, 2013, **42**, 5987–5995.
10 F. Bonaccorso, Z. Sun, T. Hasan and A. C. Ferrari, *Nat. Photonics*, 2010, **4**, 611–622.
11 L. Xie, L. Jiao and H. Dai, *J. Am. Chem. Soc.*, 2010, **132**, 14751–14753.
12 J. S. Burgess, B. R. Matis, J. T. Robinson, F. A. Bulat, F. K. Perkins, B. H. Houston and J. W. Baldwin, *Carbon*, 2011, **49**, 4420–4426.
13 H. L. Poh, F. Šaněk, Z. Sofer and M. Pumera, *Nanoscale*, 2012, **4**, 7006–7011.
14 S. Pekker, J.-P. Salvetat, E. Jakab, J.-M. Bonard and L. Forro, *J. Phys. Chem. B*, 2001, **105**, 7938–7943.
15 P. Kumar, K. Subrahmanyam and C. Rao, *Mater. Express*, 2011, **1**, 252–256.
16 E. Clemmensen, *Ber. Dtsch. Chem. Ges.*, 1913, **46**, 1837–1843.
17 M. L. Di Vona and V. Rosnati, *J. Org. Chem.*, 1991, **56**, 4269–4273.
18 J. H. Brewster, *J. Am. Chem. Soc.*, 1954, **76**, 6364–6368.
19 V. H. Pham, H. D. Pham, T. T. Dang, S. H. Hur, E. J. Kim, B. S. Kong, S. Kim and J. S. Chung, *J. Mater. Chem.*, 2012, **22**, 10530–10536.

20 W. Hummers and R. Offeman, *J. Am. Chem. Soc.*, 1958, **80**, 1339–1339.

21 U. Hofmann and A. Frenzel, *Kolloidn. Zh.*, 1934, **68**, 149–151.

22 B. C. Brodie, *Ann. Chim. Phys.*, 1860, **1860**, 466–472.

23 L. Staudenmaier, *Ber. Dtsch. Chem. Ges.*, 1898, **31**, 1481–1487.

24 C. K. Chua and M. Pumera, *Chem. Soc. Rev.*, 2014, **43**, 291–312.

25 C. K. Chua, Z. Sofer and M. Pumera, *Chem. – Eur. J.*, 2012, **18**, 13453–13459.

26 M. Mayer, *Nucl. Instrum. Methods Phys. Res., Sect. B*, 2014, **332**, 176–180.

27 J. Saarilahti and E. Rauhala, *Nucl. Instrum. Methods Phys. Res., Sect. B*, 1992, **64**, 734–738.

28 A. C. Ferrari, J. C. Meyer, V. Scardaci, C. Casiraghi, M. Lazzeri, F. Mauri, S. Piscanec, D. Jiang, K. S. Novoselov, S. Roth and A. K. Geim, *Phys. Rev. Lett.*, 2006, **97**, 187401.

29 L. G. Cancado, K. Takai, T. Enoki, M. Endo, Y. A. Kim, H. Mizusaki, A. Jorio, L. N. Coelho, R. Magalhaes-Paniago and M. A. Pimenta, *Appl. Phys. Lett.*, 2006, **88**, 163106.

30 P. Šimek, Z. Sofer, O. Jankovský, D. Sedmidubský and M. Pumera, *Adv. Funct. Mater.*, 2014, **24**, 4878–4885.